

Multiscale modelling of microstructure formation in polymer casting

T. Pitkänen, S. Majaniemi, T. Ala-Nissila

A data bank approach to multi-scale modelling of polymer solidification under flow and holding conditions is presented with applications to injection molding. The latent heat of solidification, which acts as an input parameter for large scale simulations, is determined as a function of different process dependent parameters such as the flow speed, supersaturation and geometric properties including the seed density of emerging spherulitic microstructures. Supersaturation and flow velocities are obtained from the larger scale simulation code as input values as function of which the released latent heat can be obtained from the pre-computed data bank thereby offering a possibility to circumvent the spatial and temporal coarse-graining problem associated with large scale simulations.

1 Introduction

Real plastic parts produced using injection molding range in size from $\sim 1m$ (car bumpers) to $\sim 10^{-1}m$ (mobile phone covers) and to even smaller scales (thin directions in miscellaneous small parts). Usually plastic parts are thin, meaning that the dimensions perpendicular to the flow direction are roughly a hundred times smaller than the numbers given above. The narrowness of the flow channel allows for the Hele-Shaw fluid flow approximation (Dantzig and Tucker III (2001)) to be used in the larger scale simulation of the mold filling utilizing the model to be presented in Sect. 2.1. Even with this approximation the mesh used in the mold fill-up simulation is too coarse to be able to incorporate any features and effects of the microstructure such as spherulites. A qualitative view of the solidification dynamics and microstructure formation are presented Fig. 1 depicting a model cavity.

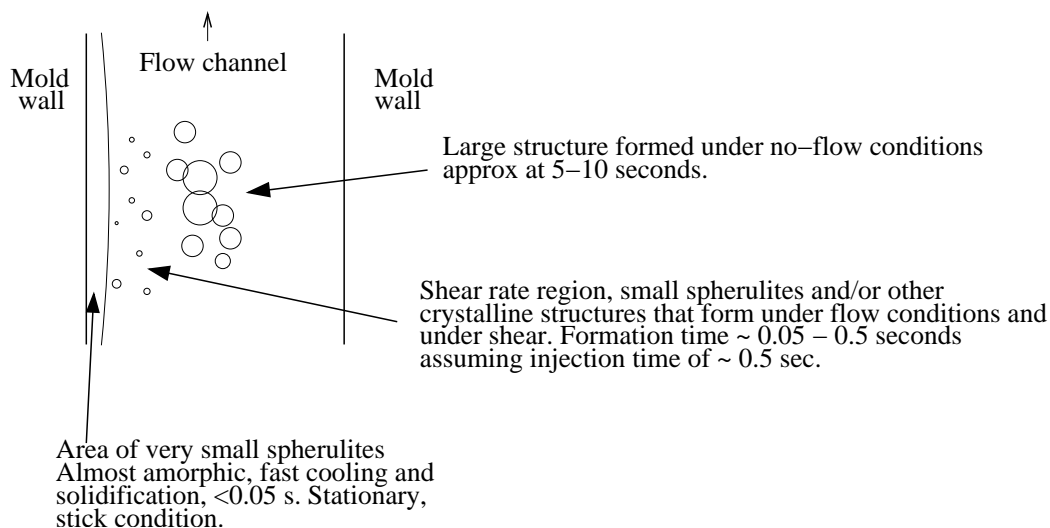


Figure 1: Rough estimates on size distributions of emerging microstructure and associated time scales

Production of latent heat is an important factor in understanding the solidification of polymer melt. In injection molding the raw polymer, usually in the form of pellets, is first ground to powder and then heated to melting temperature that is approximately between $50 - 300$ ° C depending on raw plastics used. The highly viscous polymer melt is then injected into the mold under pressure of $\sim 500 - 1500$ bar. Despite high pressure the flow of the melt is laminar and the filling of the mold lasts on the order of one second depending on the size of the mold.

Typical injection speeds are around 100 - 200 mm/s. Molds are sometimes cooled with water and parts produced are usually ejected from the mold after 10 - 20 seconds (curing time). Depending on the polymer used the molded products shrink between 0.1 - 2 % relative to the volume of mold cavity. These estimates are based on plastic materials datasheets at www.campusplastic.com (2009).

While in the molding process there are various microscopic phenomena present whose quantitative understanding is missing at present, we concentrate on the effect of microstructure on the local latent heat production in this article. This choice is motivated (1) by the fact that thermal history is important for various macroscopic phenomena e.g. local strains, and (2) by the fact that the latent heat offers a simple test bench for testing the data bank philosophy for coupling of multi-scale models.

2 Model

The main challenge in modeling polymer injection molding is the existence of multiple, widely separated time and length scales. On the largest scale, there is the injection mold which is of macroscopic size (up to the meter scale) and gets filled in time scale of seconds. On smaller scales, there is the microstructure of the solidifying polymer melt, which should be modeled on the sub-micrometer scale, and develops on the time scale of $10^{-6} - 10^{-9}$ seconds. Similarly, the difference in the time steps of the large scale and small scale numerical solvers can be in the range of three to six orders or magnitude. It is thus evident that at present it is impossible to construct a single computational model, which could span all these scales within a single simulation run. Thus, we propose here to apply a data bank approach, where simulation data from the small scales are computed and stored into a look-up table, and then fed into a large-scale model. To this end, we first construct a large-scale continuum model appropriate for the molding (Sect. 2.1). This allows us to identify the relevant fields and physical parameters, which have to be computed from a more microscopic model. We then propose a model appropriate for solidification on the micron scale based on the phase-field approach to distinguish between the melt and solid phases of the polymer. This is done in Sect. 2.2. The coupling between the microscopic and macroscopic models utilizes the data bank ideology to be explained in Sect. 3. Finally, By using a simple 2D test case in Sect. 4 we demonstrate how the data from the phase-field model can be used in the large scale simulations.

2.1 Large scale model

On large scales the polymer melt flowing into the mold can be described with the following balance equations:

$$\frac{\partial \tilde{\rho}}{\partial t} + \nabla \cdot (\tilde{\mathbf{v}} \tilde{\rho}) = 0 ; \quad (1)$$

$$\tilde{\rho}(c_p \frac{\partial \tilde{T}}{\partial t} + \tilde{\mathbf{v}} \cdot \nabla \tilde{T}) = \tilde{Q}(\tilde{T}(\mathbf{x}, t)) + \nabla \cdot (\lambda \nabla \tilde{T}) + \eta \tilde{\gamma}^2 ; \quad (2)$$

$$\tilde{Q}(\tilde{T}(\mathbf{x}, t)) \equiv \begin{cases} 0 & \text{for } \tilde{T} < \tilde{T}_m \\ \text{const.} & \text{for } \tilde{T} \geq \tilde{T}_m \end{cases} \quad (3)$$

$$\tilde{\rho}(\frac{\partial \tilde{\mathbf{v}}}{\partial t} + \tilde{\mathbf{v}} \cdot \nabla \tilde{\mathbf{v}}) = -\nabla \tilde{p} + \eta \nabla^2 \tilde{\mathbf{v}} , \quad (4)$$

where $\tilde{\rho}$ is the density of the melt, $\tilde{\mathbf{v}}$ is the flow velocity, \tilde{p} is the pressure, \tilde{Q} is the rate of latent heat production, η the viscosity, $\tilde{\gamma}$ shear rate, \tilde{T} temperature and \tilde{T}_m the melting temperature. The \sim -sign on top of these variables emphasizes that they are defined and used on the large scales, that is the appropriate time and space scales to simulate the filling of the mold cavity. The first equation represents the mass balance, the second is the heat equation and the fourth determines the momentum balance in the system. In some commercial simulation softwares the latent heat source \tilde{Q} is simply treated as constant during phase transformation whenever the local temperature \tilde{T} drops below the melting temperature as formalized in Eq. (3). We aim to produce the latent heat from more microscopic considerations by calculating it utilizing a microstructural solidification model to be presented below.

2.2 Small scale model

When a liquid is rapidly cooled below its melting temperature it becomes thermodynamically metastable and after nucleation occurs the liquid, or in this the case polymer melt, becomes unstable and solidification process begins. This phenomenon can be described via the time-dependent Ginzburg-Landau formalism, or more specifically by the so called Model C under the classification of Hohenberg and Halperin (1977). These types of models are also called phase-field models because they include one or more order-parameter fields, or phase fields, that describe the behavior of the degree of order (such as crystallinity) of the system. In this paper we utilize a phase field model originally developed to describe solidification in metals and formation of dendritic microstructure. The model includes two primary fields, the phase field $\phi(\mathbf{x}, t)$ and the dimensionless temperature field $u(\mathbf{x}, t) = c(T(\mathbf{x}, t) - T_m)/L$ where $T(\mathbf{x}, t)$ is local temperature, c is specific heat, T_m is melting temperature and L is the latent heat per unit volume. The phase field is an order parameter field that describes the solid ($\phi = 1$), the liquid ($\phi = -1$) phases and intermediate values of ϕ describe varying degrees of solidification of the polymer melt. Of course, polymers do not form a perfect crystal upon solidifying and therefore one has to be careful about the meaning of the order parameter. Instead of saying that $\phi = +1$ corresponds to the crystal it would be more appropriate to say that for polymers this value corresponds to the polymer solid characterized with its mean porosity in the solid phase. The liquid regions ($\phi = -1$ for metals) could give a measure of amorphous regions having more liquid like symmetries. More sophisticated phase field models described by more faithful free energies for polymeric systems can overcome these interpretational ambiguities and will be studied in future work.

The microscopic phase field and the temperature fields evolve according to the following coupled equations (see e.g. Langer (1980)),

$$\frac{\partial \phi(\mathbf{x}, t)}{\partial t} + \nabla \cdot (\phi(\mathbf{x}, t)\mathbf{v}) = -\frac{1}{\tau H} \frac{\delta F(\phi, T)}{\delta \phi} \quad (5)$$

$$\frac{\partial u(\mathbf{x}, t)}{\partial t} + \nabla \cdot (u(\mathbf{x}, t)\mathbf{v}) = Q(\mathbf{x}, t) + \nabla \cdot (\alpha \nabla u(\mathbf{x}, t)) \quad (6)$$

$$Q(\mathbf{x}, t) \equiv \frac{1}{2} \frac{\partial \phi(\mathbf{x}, t)}{\partial t}. \quad (7)$$

Eq. (5) is the phasefield equation for the polymer order parameter and Eq. (6) is the *small scale* temperature flow equation (which is solved separately from the large scale temperature \tilde{T}). The convective velocity is denoted by \mathbf{v} and will be discussed in more detail at the end of this section. In Eq. (5) τ is the characteristic time scale of the model and H is the nucleation barrier in the free energy F . In Eq. (6) α is the thermal conductivity and $Q(\mathbf{x}, t)$ is the pointwise rate of latent heat production on the microscopic scales. The functional derivative of the free energy $\delta F(\phi, T)/\delta \phi$ corresponds to chemical potential that drives the time evolution of the phase field.

For the free energy we choose the standard form,

$$F[\phi, T] = \int \left\{ \frac{1}{2} \epsilon |\nabla \phi|^2 + f(\phi(\mathbf{x}, T)) \right\} d^3 \mathbf{x} \quad (8)$$

where ϵ sets the scale of the surface tension. Free energy density $f(\phi(\mathbf{x}, T))$ has the general form,

$$f(\phi(\mathbf{x}, T)) = f_L(T_m) + H g(\phi) + \frac{(T - T_m)L}{T_m} P(\phi). \quad (9)$$

The interpolating polynomials $g(\phi)$ and $P(\phi)$ are taken from Karma and Rappel (1996) $g(\phi) = -\frac{1}{2}\phi^2 + \frac{1}{4}\phi^4$, resulting in a double well structure, and $P(\phi) = \phi - \frac{2}{3}\phi^3 + \frac{1}{5}\phi^5$. After substituting these polynomials into the free energy, Eq. (5) for the phase field evolution becomes

$$\frac{\partial \phi(\mathbf{x}, t)}{\partial t} = -\frac{1}{\tau H} \left[\epsilon^2 \nabla^2 \phi + H \frac{dg(\phi)}{d\phi} - \frac{(T - T_m)L}{T_m} \frac{dP(\phi)}{d\phi} \right] - \nabla \cdot (\phi(\mathbf{x}, t)\mathbf{v}) \quad (10)$$

$$= \frac{1}{\tau} \left[\frac{\epsilon^2}{H} \nabla^2 \phi + \phi - \phi^3 - \Lambda u(\mathbf{x}, t)(1 - \phi^2)^2 \right] - \nabla \cdot (\phi(\mathbf{x}, t)\mathbf{v}) \quad (11)$$

with the constant $\Lambda = \frac{L^2}{cT_m H}$. The width W of the interface between solid and liquid is determined from following equation: $W^2 = \epsilon^2 H$. When time and space are rescaled dimensionless with $x \rightarrow x/W$ and $t \rightarrow t/\tau$ respectively one ends up with the equations

$$\frac{\partial \phi(\mathbf{x}, t)}{\partial t} = \nabla^2 \phi + \phi - \phi^3 - \Lambda u(\mathbf{x}, t)(1 - \phi^2)^2 - \nabla \cdot (\phi(\mathbf{x}, t)\mathbf{v}) \frac{\tau}{W} \quad (12)$$

$$\frac{\partial u(\mathbf{x}, t)}{\partial t} = Q + \bar{D} \nabla^2 u(\mathbf{x}, t) - \nabla \cdot (u(\mathbf{x}, t)\mathbf{v}) \frac{\tau}{W} \quad (13)$$

$$Q = \frac{1}{2} \frac{\partial \phi(\mathbf{x}, t)}{\partial t}. \quad (14)$$

Solving of the Eqs. (12)- (14) is now possible once the supersaturation Δ (the initial difference of the large scale temperature field from the melting/freezing point),

$$\Delta \equiv u(\mathbf{x}, t = 0) \quad (15)$$

and the constants Λ and $\bar{D} = \alpha\tau/W^2$ are given numerical values. The temperature coupling of the small scale model with the large scale one is established via the initial condition (15) for the supersaturation Δ , which is needed for the computation of the temperature flow equation (13). Since the large scale simulation mesh (Fig. (2a)) has a cell size which represents the entire small scale simulation domain (Fig. (2c)), the large scale temperature $\tilde{T}(t + \delta t_i)$ will be a constant in the entire small scale simulation domain, and will thus set the constant supersaturation (initial condition) for the smaller scale simulation through $\Delta \equiv \tilde{T}(t + \delta t_i) - \tilde{T}(t)$. In order to use Eq. (15) for the small scale simulation we only need to know how much above the freezing point the local temperature of a given cell in the large scale simulation rose in the given large scale simulation time step δt_i . Of course, for polymers we should keep in mind the ambivalence related to the concept of freezing/melting temperatures T_m as compared to real crystals.

Finally, let us consider the velocity coupling between the two scale regimes which manifests itself through the convective terms $\nabla \cdot (\phi(\mathbf{x}, t)\mathbf{v})$ in Eq. (12) and $\nabla \cdot (u(\mathbf{x}, t)\mathbf{v})$ in (13). In contrast to the basic Model C, we have added these convective terms to mimic the effects of fluid flow through the solidifying matrix. The velocity field \mathbf{v} is related to the large scale velocity field $\tilde{\mathbf{v}}$ in the following way:

$$\mathbf{v}(\mathbf{x}, t) \equiv (1 - \phi(\mathbf{x}, t)) \tilde{\mathbf{v}}. \quad (16)$$

In other words, even though $\tilde{\mathbf{v}}$ is constant within the microscale simulation domain, \mathbf{v} acquires spatial and temporal dependence because of the phase field prefactor $(1 - \phi(\mathbf{x}, t))$ appearing on the right hand side of Eq. (16). The prefactor $(1 - \phi(\mathbf{x}, t))$ was added to kill the velocity field in the solidified regions where $\phi = +1$. This approximation is rather crude, though, because it does not account for blocking the fluid flow in the liquid regions (or in porous amorphous regions) which are completely surrounded by solidified areas. Nevertheless, the definition utilized above is good enough for testing the data bank philosophy. It should be noted that Eq. (12)- (14) could also be derived through a suitable analytic coarse graining procedure from even more microscopic equations for polymer flow such as those given in Ref. Ohta et al. (1993).

2.3 Estimation of parameters for small scale model

Equations of type (12)- (14) have been used to simulate the solidification of metals, e.g. Nickel in Nestler et al. (2005), and from such calculations it can be estimated that $v_{ave, Ni} \sim 100m/s$ and $W_{Ni} \sim 7 * 10^{-10}m$. Where v_{ave} is the approximate steady state metallic dendrite growth speed. It is plausible to assume that the interfacial width of the solidifying lamellar and/or spherulitic polymer front W_P is larger than for metals whereas the crystal growth speed is lower. To allow for some latitude for different polymeric materials we introduce two scale factors B_1 and B_2 . We can write for polymer $W_P \sim B_1 W_{Ni}$ and $v_{ave, P} \sim B_2 v_{ave, Ni}$, where we could have, for example $B_1 = 10 - 1000$ and $B_2 = 0.1 - 0.001$. If we choose values $B_1 = 100$ (making the polymeric interface width about hundred times larger than the metallic which is atomistic) and $B_2 = 0.01$ (making the front move about hundred times slower than the metallic one) we get $W_P \sim B_1 W_{Ni} = 7 * 10^{-8}m$, $v_{ave, P} \sim B_2 v_{ave, Ni} = 1m/s$ and the flow velocity for dimensionless input parameter value of e.g. $\tilde{v}_x = 0.2$ gives for real flow speed $v_x = \tilde{v}_x W_P / \tau_P \sim \tilde{v}_x * B_2 * v_{ave, Ni} = 0.2m/s$ which compares to typical injection flow speeds of $\sim 0.1m/s$. Where $\tau_P \sim (B_1/B_2)\tau_{Ni} \sim 10^{-8}$ is the typical time scale for polymers. The values used in our simulation for the phase field domain read as follows: domain size $N_x = N_y = 400$, and dimensionless x-co-ordinate $\Delta x = 0.4$ which corresponds to $L \sim N_x \Delta x W_P \sim N_x \Delta x B_1 W_{Ni} \sim 10^{-5}m$ in the real world units. This can of course be changed by changing the scale factors B_1 and B_2 depending on materials to be modelled.

3 Multiscale coupling: look-up table for latent heat

In Fig. 2 there is a schematic presentation of the idea how the effects of the microstructure information on the latent heat Q production can be transmitted to large scale simulation software via the data bank which is basically a large look-up table. The Finite Element (FEM) mesh for the simulation domain of the large scale model is depicted in Fig. 2a. The idea is to simulate the solidification of polymers with equations (12)-(14) within the small scale simulation box (subfigure 2c), which has the size of a single unit cell of the large scale mesh. For the small scale simulation (phase field model for the microstructure) the unit cell of the large scale mesh is further subdivided into smaller cells using a finer grid. Of course, it would be too time consuming to perform this type of fine-graining for each of the cells of the large scale computational domain which would also provide the boundary conditions for the small scale simulation such as the average supersaturation and the velocity $\tilde{\mathbf{v}}$. Therefore, we resort to a data bank, which is like a representative unit cell. In other words, we perform the small scale simulation in a computational domain representing a single large scale unit cell using Eq. (12)- (14). For each run we choose different input parameters (such as $\tilde{\mathbf{v}}$ and Δ). The simulation results for the latent heat will be stored in the data bank for this entry. The process is repeated for many different values of the input parameters. Once the data bank has sufficiently many entries, it can be coupled with the large scale simulation program as follows. After a single large scale simulation time step δt_i is completed the large scale velocity field and the large scale temperature field have certain values. To obtain the corresponding latent heat produced during the large scale time interval we read the value of Q from the data bank whose entries give the closest match to the actually realized values of the large scale simulation for Δ and \mathbf{v} . In this way, in each large scale cell we can read off the closest corresponding value for Q from the data bank of the representative volume element for the entry (Δ, \mathbf{v}) characterizing that particular large scale element.

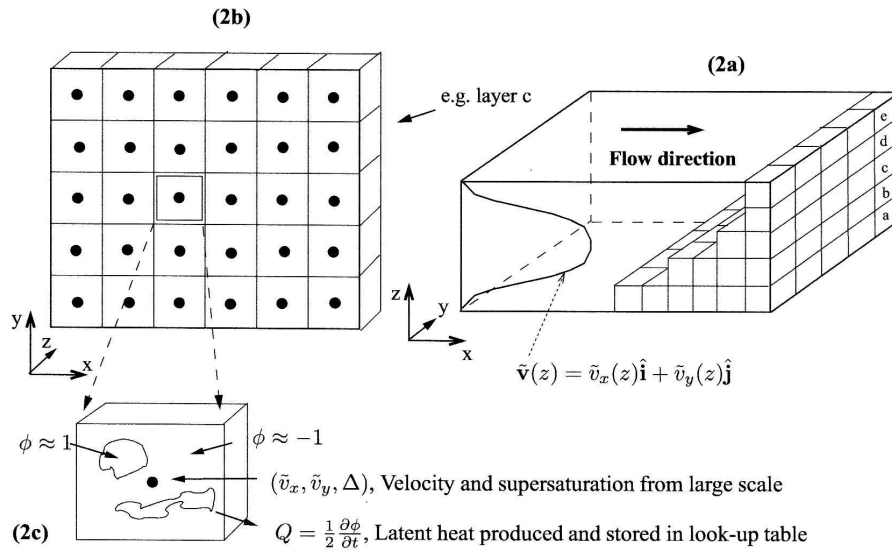


Figure 2: Small scale simulation box within the large scale mesh. Fig. (2a) shows the large scale mesh and an evolving flow velocity distribution on the left. Fig. (2b) depicts one layer of large scale simulation elements and Fig. (2c) is the blow-up of a single mesh cell within the layer. The small scale simulations of the phase field model determined by Eqs. (12)- (14) are done within this representative volume element for many different values of the large scale velocity field $\tilde{\mathbf{v}}$ and other parameters. In this figure a 3D flow situation has been illustrated. In Sect. 4 the simulations have been performed in 2D.

At the moment we have simulated the small scale Eqs. (12)- (14) and calculated the latent heat for various values of Δ , $\mathbf{v}(z)$ and n_s , where n_s is the seed density of initial solid nuclei per unit of area. The resulting latent heat is averaged over the small scale simulation domain spatially and stored in the look-up table: $Q = Q(\Delta, \mathbf{v}(z), n_s, t)$. The large scale \tilde{Q} can be related to Q through the following equation:

$$\tilde{Q}(\mathbf{x}, t) \equiv \langle Q(\Delta, \mathbf{v}, n_s) \rangle, \quad (17)$$

where the spatial average $\langle \cdot \rangle$ is taken over the volume of the representative element. It should be noted that \tilde{Q} above is not simply given as a function of the large scale temperature $\tilde{T}(\mathbf{x}, t)$ anymore, in contrast to Eq. (3). Rather, $\tilde{T}(\mathbf{x}, t)$ is only used to set the initial supersaturation for the representative volume element through Eq. (15)

4 Results

We have performed simulations of the small scale Eqs. (12)- (14) in 2D box of size 400x400 with the following input parameters: flow velocity $\mathbf{v} = v_x \hat{\mathbf{i}} + v_y \hat{\mathbf{j}} \in [(0.0; 0.0), (0.1; 0.0), (0.2; 0.0), (0.3; 0.0), (0.4; 0.0)]$, supersaturation $\Delta \in [-0.2, -0.3, -0.4, -0.48, -0.55]$, space discretisation $\Delta x = \Delta y = 0.4$, simulation time step $\Delta t = 0.0005$ and parameter $\Lambda = 3.19$. We have simulated up to $n_t = 2.8 \cdot 10^6$ time steps (in simulation time $t = \Delta t \cdot n_t = 2.8 \cdot 10^6 \cdot 0.0005 = 1400$) in order to be sure that the temperature field is saturated homogeneously to zero (i.e. $T = T_m$ everywhere). The nucleation was induced artificially by setting value of the phase field to one at the seed points. The number of seeds (n_s) varied from $n_s = 1$ to $n_s = 20$. The spatial distribution of the seeds in the initial configurations was varied as well.

As can be seen from Figure (3) the latent heat production takes place primarily before simulation time $t = 500$. In Figure (3) we show the latent heat production $Q(v_x, t)$ as function of simulation time t and x-component of the flow velocity v_x (y-velocity is zero all the time) for seed numbers $n_s = 2$ (plot on the left in Fig. (3)), $n_s = 5$ (center) and $n_s = 20$ (right) respectively. As the number of seeds increases the influence of the flow velocity decreases and for $n_s = 20$ all the Q -curves are almost identical. This collapse of the $Q(v_x, t)$ -curves with constant supersaturation onto a single master curve independent of velocity is reminiscent of the scaling behavior seen in other systems (Greenwood et al. (2004)). With small n_s the solidifying front has more room to grow before it encounters another solidification front. This means that the homogenisation of the temperature field takes longer for configurations with smaller number of seeds. Thus, for low seed numbers solid is being formed during a longer time period than with higher seed number, which can be seen from Fig. (3) where the time it takes to reach a zero latent heat production rate decreases for increasing seed number. We observed that the configuration of the seeds with low seed numbers e.g. $n_s = 2$, affects the behavior of $Q(v_x, t)$ as a function of time but doesn't change the total Q integrated over the whole simulation time. This behavior (not shown in the current figures) is geometry related and disappears with higher seed numbers, for example with $n_s = 20$ the shape and total amount of latent heat produced was invariant to (randomly distributed) configuration of the seeds.

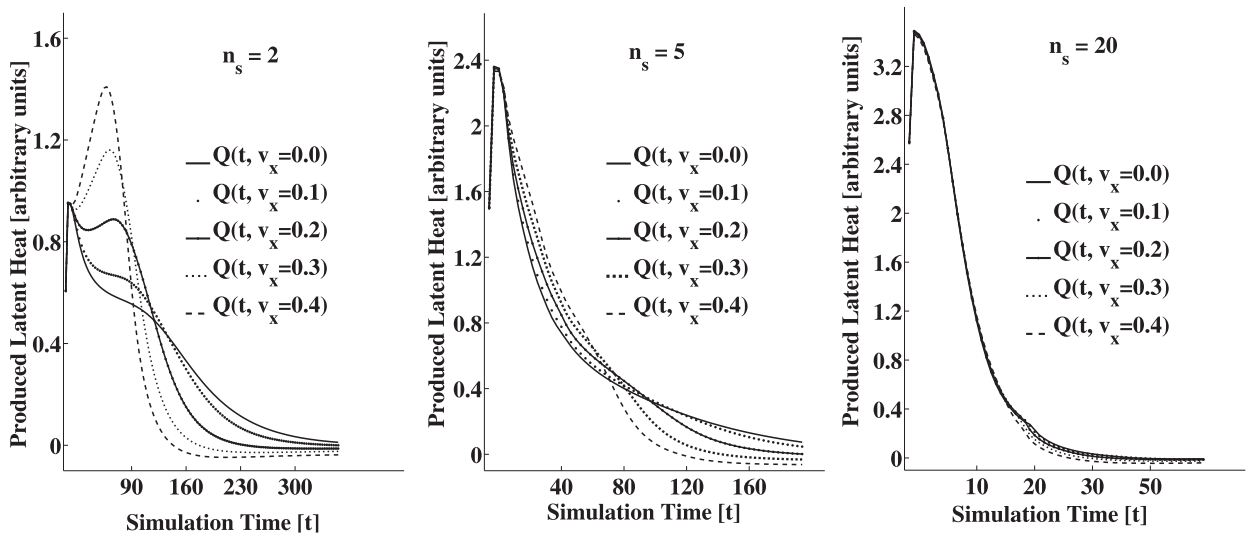


Figure 3: Latent heat produced with varying initial seed number: $n_s = 2$ (left), $n_s = 5$ (center) and $n_s = 20$ (right)

In Figures (4) - (6) we present snapshots of phase field configurations at different times corresponding to computed latent heat values presented in Figures (3) and (7). In the snapshots the blue color corresponds to liquid ($\phi \sim -1$) and the red color to solid ($\phi \sim 1$) areas. For example in Fig. (5) the subfigure (A) is the starting configuration for the five seed simulation ($t=0$) with zero flow velocity, subfigure (B) is the situation after $200/(\Delta t) = 4 \cdot 10^5$ time steps, subfigure (C) depicts the initial condition with flow velocity $v_x = 0.3$ and $n_s = 5$ and subfigure (D) presents the situation after $4 \cdot 10^5$ time steps. The same nomenclature applies for Figures (4) and (6). Note that simulation times differ between aforementioned figures. The effect of the flow velocity can be seen as a distortion of solidifying areas. The growth of solid areas is stronger against the direction of the velocity (direction of negative x-axis) in Figures (4) - (6).

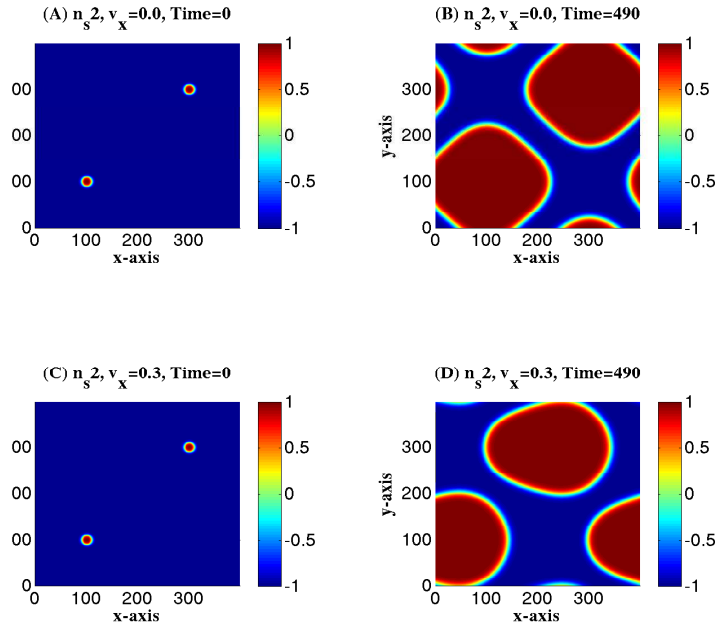


Figure 4: Snapshots of the phase field configuration with two diagonally placed seeds at two different times (left $t = 0$, right $t = 490$) and for two different velocities (A and B $v_x = 0.0$, C and D $v_x = 0.3$)

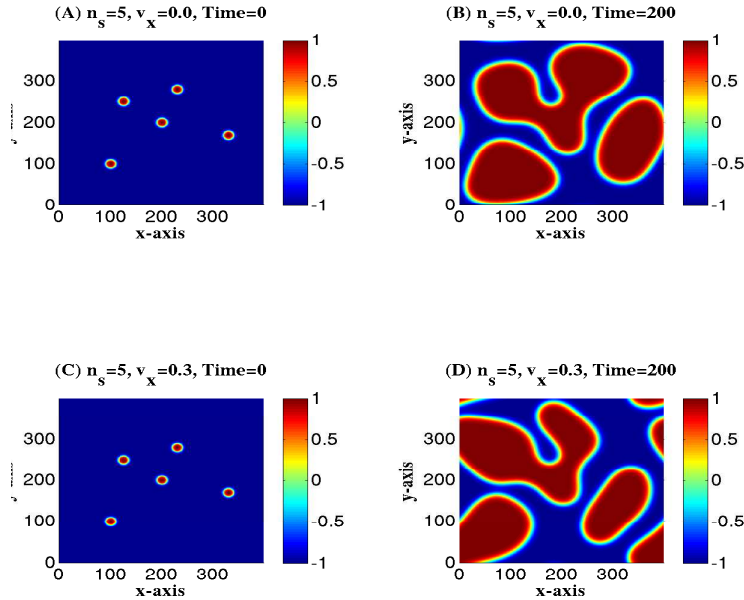


Figure 5: Snapshots of the phase field configuration with five seeds at two different times (left $t = 0$, right $t = 200$) and for two different velocities (A and B $v_x = 0.0$, C and D $v_x = 0.3$). The non zero flow velocity effects the morphology of the solidified areas somewhat more strongly in Fig. (6 D) than in Fig. (5 D).

In Figure (7) we show the behavior of $Q(\Delta, t)$ with zero flow velocity v_x for seed numbers $n_s = 5$ on the left and $n_s = 20$ on the right as a function of the supersaturation Δ . If the latent heat of solidification is taken to be

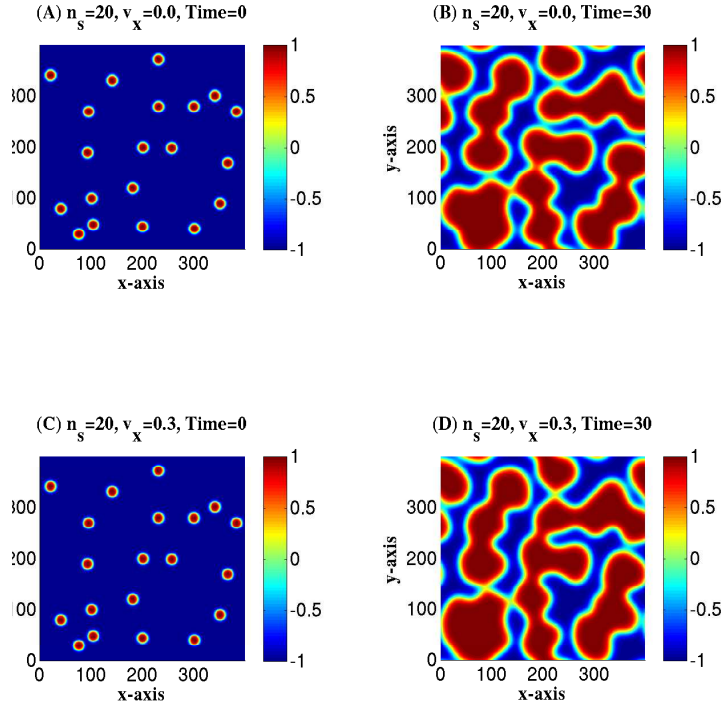


Figure 6: Snapshots of the phase field configuration with twenty seeds at two different times (left $t = 0$, right $t = 30$) and for two different velocities (A and B $v_x = 0.0$, C and D $v_x = 0.3$)

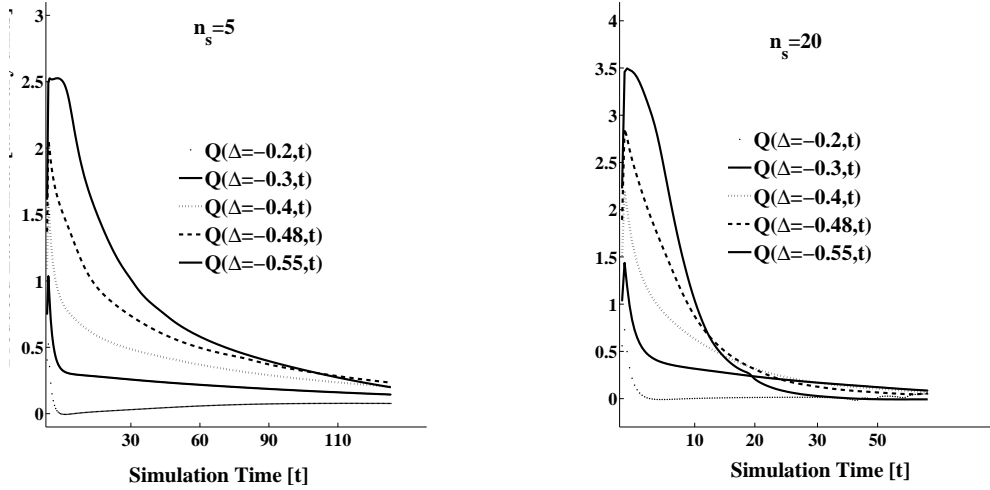


Figure 7: Latent heat produced with varying supersaturation Δ for $n_s = 5$ (left) and $n_s = 20$ (right)

between $L = 0.5 \cdot 10^8 - 3 \cdot 10^8 J/m^3$ and specific heat between $c = 1 \cdot 10^6 - 2 \cdot 10^6 J/m^3$ we get for the physical supersaturation $\Delta = T - T_m \sim L/c\Delta = 20K$ for choices $L = 2 \cdot 10^8 J/m^3$, $c = 10^6 J/m^3$ and $\Delta = 0.4$. For the curves in Figure (7) the total latent heats Q_{TOT} are calculated by integrating over time and simulation box and normalizing with the Q_{TOT} value for $\Delta = -0.55$:

$$Q_{TOT} = \frac{\iint_{t,A} Q(\Delta, \mathbf{v} = 0, n_s) dadt}{\iint_{t,A} Q(\Delta = -0.55, \mathbf{v} = 0, n_s) dadt} \quad (18)$$

where A is the area of the 2D simulation box and the time integration is over the whole simulation time. Table (1)

shows the normalized latent heats in dimensionless units for different supersaturations Δ and seed numbers n_s . Unlike for the velocities increasing the number of seeds (per unit area) does not force the latent heat to collapse onto a master curve in the same manner as in Fig. (3) ($n_s = 20$)

Seed number n_s	Q_{TOT} as function of supersaturation Δ [simulation units]				
	$\Delta = -0.2$	$\Delta = -0.3$	$\Delta = -0.4$	$\Delta = -0.48$	$\Delta = -0.55$
5	0.075	0.299	0.522	0.757	1.000
20	0.041	0.372	0.619	0.825	1.000

Table 1: Total latent heat Q_{TOT} as function of supersaturation Δ . Latent heats are normalized so that for the largest supersaturation $\Delta = -0.55$ the total time and space averaged $Q_{TOT} = 1.000$

From the values of Table (1) it is observed that the lowest supersaturation of $\Delta = -0.2$ produces almost an order of magnitude less latent heat than higher supersaturations. The driving force of the temperature difference of $\sim 10K$ in the case of $\Delta = -0.2$ is barely able to solidify the supersaturated (undercooled) liquid. For smaller supersaturations modified numerical schemes will be considered in future work.

5 Conclusions and future work

We have demonstrated the plausibility of the data bank approach to multi-scale modelling of polymer solidification using 2D phase field simulations. We have presented a coupling mechanism between a large scale flow simulation model and the small scale microstructural evolution model by parameterizing the data bank in terms of the supersaturation, melt velocity and the seed density. These parameters, which act as entries of the data bank, are obtained directly from the large scale simulation program (Δ and \mathbf{v}) or can be estimated indirectly (n_s) e.g. from the distance of the mold walls and some probabilistic arguments. The information transfer between the macro and micro scales is two directional: The data bank entries are obtained from the large scales and the content of the data bank (Q corresponding to the closest match of the entries) is fed back into the large scale simulation program at fixed time intervals, which in the simplest case is the length of a single time step δt_l of the large scale program. The way of choosing the size of the optimal δt_l will also be considered in future work.

Both the phase field model and the construction of the data bank can be improved considerably. In the future work we will consider different forms for the free energy, which will take the polymeric nature of the melt better into account. The coupling of the velocity field can also be improved. As for the data bank, its parametrization can be enlarged by taking into account time dependent changes in the input parameters. If the matching of the time scales of the small scale and large scale models requires history data to be stored, the size of the data bank grows very rapidly, and we have to start considering other ways of compressing the information. One possibility is to try to find universal scaling functions and dimensionless combinations of fields such as presented by Greenwood et al. (2004) for spacing length selection in directional solidification. In the present work, we note that increasing seed density causes a similar collapse of the time dependent latent heat production onto a single master curve thereby making the velocity a redundant parameter at high enough densities where sufficient self-averaging takes place.

6 Acknowledgements

M.Sc. Timo Pitkänen and Dr. Sami Majaniemi have received funding for this work from the Finnish Funding Agency for Technology and Innovation (Tekes) project PhaseField. We would also like to thank Dr.-Ing. P.F. Filz, Dr. rer. nat. K. Weibelhaus and T. Ture for useful discussions.

References

- Dantzig, J. A.; Tucker III, C. L.: *Modeling in Materials Processing*. Cambridge University Press, UK (2001).
- Greenwood, M.; Haataja, M.; Provatas, N.: Crossover scaling of wavelength selection in directional solidification of binary alloys. *Phys. Rev. Lett.*, 93, (2004), 246101.
- Hohenberg, P. C.; Halperin, B. I.: Theory of dynamic critical phenomena. *Reviews of Modern Physics*, 49 No. 3, (1977), 435–479.
- Karma, A.; Rappel, J.-W.: Phase field method for computationally efficient modelling of solidification with arbitrary interface kinetics. *Phys. Rev. E*, 53, 4, (1996), 3017.

Langer, J. S.: Instabilities and pattern formation in crystal growth. *Rev. Mod. Phys.*, 52, (1980), 1.

Nestler, B.; Danilov, D.; Galenko, P.: Crystal growth of pure substances: Phase-field simulations in comparison with analytical and experimental results. *J. Comp. Phys.*, 207, (2005), 221–239.

Ohta, T.; Enomoto, Y.; L., H. J.; Doi, M.: Anomalous rheological behavior of ordered phases of block copolymers. *Macromolecules*, 26, (1993), 4928–4934.

www.campusplastic.com: (2009).

Address: M.Sc. Timo Pitkänen, Dr. Sami Majaniemi and Prof. Tapio Ala-Nissilä, Department of Applied Physics, COMP center of excellence, Helsinki University of Technology, P.O. Box 1100, FIN-02015, TKK, Finland.
emails: timo.pitkanen@tkk.fi, majaniemi@physics.mcgill.ca,
tapio.ala-nissila@tkk.fi